JOURNAL OF MATERIALS SCIENCE 26 (1991) 5275–5291

As-spray-deposited structure of an Al–20Si–5Fe Osprey preform and its development during subsequent processing

J. ZHOU, J. DUSZCZYK, B. M. KOREVAAR
Laboratory for Materials Science, Delft University of Technology, Rotterdamseweg 137, 2628 Al Delft, The Netherlands

The application of the Osprey process to the fabrication of newly developed Al–20Si–X alloys is at present a subject of considerable interest. This paper reports the results of a study on the as-spray deposited structural characteristics of an Al–20Si-5Fe alloy preform and their development during subsequent hot extrusion and high-temperature exposure, by means of X-ray diffraction, differential scanning calorimetry and electron microscopy. It is shown that in the as-spray-deposited preform of the alloy an unusual increase in the lattice parameter of the aluminium matrix was detected, which persisted throughout the processing. No evidence of supersaturation in the preform aluminium matrix could be found, which is considered to be associated with the characteristics of solidification and subsequent decomposition of the hypereutectic alloy during spray deposition, this allows the extensive formation of second phases and thus a substantial decrease in the solute enrichment of the solution. A metastable intermetallic phase, identified as δ-Al_4FeSi_2, together with silicon phase, was present as the predominant dispersed phase in the preform, and its transformation into the equilibrium phase, β-Al_5FeSi, through a peritectic reaction under the equilibrium conditions, must have been effectively suppressed during the Osprey process. The δ-phase initially with a platelet shape was fragmented into short rods during the extrusion subsequent to spray deposition, while a part of this phase was transformed into the equilibrium β-phase under the combined influence of heat and deformation. The refinement of the δ-phase, on the other hand, was found to decrease its metastability and thus to promote its decomposition during subsequent annealing at 400 °C. The coexistence of the high volume fractions of the intermetallic and silicon phases in the extruded material greatly modified its restoration kinetics, resulting in a partially recrystallized microstructure, after prolonged soaking at 400 °C for 100 h. Also shown is a peculiar microstructure of the as-spray-deposited material with numerous spherical colonies of 10–20 μm, characterized by the finer silicon particles and δ-phase platelets in their interior and occasionally decorated with micropores at their peripheries. These colonies are considered to originate from the remains of very fine droplets and particles in the larger droplets, which are presolidified in flight and then partially remelted at the deposition surface. The colonies were mixed up with the rest of the microstructure and the micropores closed by applying an extrusion operation.

1. Introduction

It has generally been recognized that the Osprey process is an innovative technique of spray deposition which can be used to produce rapidly solidified, near-net-shape materials [1]. In this process, droplets are first atomized from a molten metal stream, quickly cooled by an inert gas, then deposited on a substrate, and finally built up to form a low-porosity deposit with a required shape (preform) [2]. Apparently, a unique feature of this process is that the separate steps of atomization and primary consolidation normally involved in the conventional powder metallurgy (P/M), the techniques most often used to fabricate rapidly solidified materials [3], are combined into a single operation and completed in a closed chamber with a protective atmosphere. As a result, a number of drawbacks that the powder metallurgy possesses, such as multi-step processing and easy powder contamination by oxygen and hydrogen, no longer exist [4]. The simplification in processing and thus reduction in fabrication cost are markedly in favour of the application of the Osprey process as an alternative means of producing rapidly solidified materials that generally have improved properties. Therefore, since the emergence of this process, it has attracted world-wide interest. Most of the investigations so far carried out

0022–2461/91 $03.00 + .12

have been directed toward the process control [5] and the theoretical understanding of spray-deposition fundamentals [6–10]. A thorough understanding of the structural characteristics of aluminium alloys produced by using this process and their development during subsequent engineering processing is, however, still lacking [11]. Obviously, this understanding is of great importance for ascertaining the solidification mechanisms of the process and for offering the background to the optimum processing of the materials.

In an attempt to develop this understanding, the present work was undertaken by characterizing the structures of an Al–20Si–5Fe alloy throughout a processing route from spray deposition through extrusion to high-temperature exposure that the material normally undergoes in manufacturing and service. The reason for choosing this newly developed, highly alloyed material as an application of the Osprey process is that it cannot readily be fabricated by the conventional techniques, such as casting followed by hot working, owing to the presence of undesirable, coarse silicon phase in the alloy [12]. In other words, it has to be produced by utilizing a technique involving rapid solidification. Applying powder metallurgy can provide the alloy with very attractive properties, workability, wear resistance, and thermal stability in particular, but its widespread application can be limited by its cost as a consequence of multi-step processing [4]. A success in applying the Osprey process, which is definitely much more cost-effective, will hopefully enhance the prospects of the alloy as a new material for the applications where hot strength, dimensional stability, and wear resistance are required. Primary tensile tests of the material produced by the Osprey process at room and high temperatures have shown very encouraging results [13], and thus the present work should be of help both in the alloy development and in the commercial adoption of the Osprey process.

2. Experimental procedure

The spray-deposited preform of the alloy, with a nominal composition of 20% Si, 5% Fe (wt) and balance aluminium, was provided by the Osprey Metals Ltd, UK. The preform had a cylindric disc shape with a diameter of about 150 mm. The as-received preform was first subjected to chemical analyses. Samples were taken from the preform to analyse the silicon and iron contents with atomic absorption and gravimetry methods, respectively. The results showed that the exact alloy composition of the preform was 19.52% Si, 4.3% Fe (wt) and balance aluminium. The oxygen content was also analysed with the Stroehlein OSA-MAT method, through measuring the amount of carbon monoxide formed during heating samples to a temperature of about 2000 °C. The porosity level was determined by means of pycnometry through measuring the mass and volume of prisms cut from the preform.

The preform, after being cut into cylindrical billets, was extruded at a temperature of 375 °C, a reduction ratio of 10:1 and a ram speed of 5 mm s^{-1} to be completely consolidated and shaped into rods as a semi-finished product. After extrusion, the material was cooled in air. To assess the effect of high-temperature exposure on the further structural evolution of the extruded material as possibly encountered in secondary forming and service, the extruded material was soaked at 300 and 400 °C for 100 h followed by slow cooling.

A Jeol JXA 50A scanning electron microscope (SEM) working at 25 kV was used to observe the microstructures of the material in the as-spray-deposited, as-extruded and as-annealed states on both the transverse and longitudinal sections. SEM specimens were heavily etched in a 0.5% HF reagent for about 1.5 min before being covered with a thin layer of carbon. The microstructures of the material were also examined with a Philips 400T transmission electron microscope (TEM) operating at a voltage of 120 kV. TEM disc-shaped specimens were prepared by using ion-beam thinning at a current of 0.5 mA and an inclination angle of 20°. X-ray powder diffraction (a Siemens D500-A diffractometer with a stepping-motor driving system) was performed to examine the aluminium matrix lattice and the intermetallic phases of the material in the different states. CoK_α radiation (40 kV/25 mA) was used, detections were made at 23 °C, and diffraction lines were recorded with a preset time method. To assist the structural observations, a thermal analysis of the Osprey preform was performed using differential scanning calorimetry (DSC). The thermal effects of a specimen of about 30 mg were compared with those of pure aluminium (99.99%) with a similar weight, heated at a rate of 5 °C min^{-1} in a Du Pont type 9900 DSC instrument.

3. Results and discussion

3.1. Characterization of the Osprey preform

3.1.1. Oxygen content

The chemical analysis showed that the oxygen content in the preform, being independent of sampling locations, varied between 0.01% and 0.02% (wt). Such a small amount of oxygen in the preform appears to come mainly from the retained oxygen in the melt feedstock, because additional oxidation during spray deposition should be very limited. The reason is that the short-time exposure (typically a few milliseconds) of the material in the droplet form with a high specific surface area to the surrounding protective atmosphere (nitrogen) with only a trace of oxygen does not permit extensive oxidation to occur. The measured low oxygen content in the preform clearly illustrates one of the major advantages of the Osprey process over the conventional powder metallurgy, by which it is generally difficult to prevent oxidation of loose powder particles effectively during cooling, handling and prolonged storage. The difference in oxygen content given by these two approaches is especially large for aluminium alloys, because of their strong tendency to oxidation. For example, P/M alloys with a composition similar to the present one were measured to have oxygen contents of 0.2% and 0.1% (wt) when atomized in air and in argon, respectively [4]. A direct

benefit which can be gained from the low oxygen content is that subsequent consolidation can be immediately and more easily conducted, because in this case there is no need to eliminate the adsorbed hydrogen, which always accompanies oxides, by applying a degassing treatment, or to apply a very large deformation to break up and redistribute tenacious oxide stringers in order to produce a coherent structure. Furthermore, improvement of such properties as fatigue strength and fracture toughness, that are sensitive to oxide inclusions, can be expected.

3.1.2. Aluminium matrix lattice

An X-ray diffraction (XRD) line from the aluminium matrix of the as-spray-deposited material is shown in Fig. 1, and compared with that from pure aluminium. The broadening of the reflection peak can easily be noted, which implies an alteration in crystallite size and the presence of micro-strains in the aluminium matrix of the preform. In general, two major factors can be considered which contribute to the line broadening of the aluminium matrix of Al–Si based alloys, in addition to instrumental conditions, specimen sizes, etc. The first one is the difference in atomic volume between silicon in dissolved and precipitated forms. If this factor was involved, the precipitation of silicon from the aluminium matrix would result in the relaxation of the micro-strains and thus a change in the breadth of diffraction lines. The examination of the matrices of the material, having undergone extrusion where precipitation was expected to occur, however, showed no further change in the breadth of diffraction lines at the half maximum [13]. This means that the first factor is not significant, or even not existent in the present case. The second factor considered to result in the diffraction line broadening is the large difference in thermal expansion coefficient between the aluminium matrix and the dispersed silicon phase, which creates tensile strains in the matrix lattice during cooling from a high temperature [14]. Owing to the relatively slow cooling of the Osprey process over the temperature range of solidification, a high volume fraction of silicon phase (about 15%) was formed. During further cooling to room temperature, micro-strains were developed in the aluminium matrix of the material and thus diffraction line broadening occurred. Because the subsequent extrusion did not produce an increased amount of silicon phase, which has been confirmed by the DSC analysis and will be described later, the micro-strains and thus the line broadening remained unchanged.

Fig. 1 also shows a shift of the diffraction line toward a lower angle, indicating an increase in the average lattice parameter of the aluminium matrix of the preform. Calculated from the {331} reflection, the average lattice parameter was 0.03% larger than that of pure aluminium ($a = 0.404\,94$ nm, ASTM card 4-0787). This result may be surprising at first sight, because the dissolved atoms in the alloy, silicon and iron, both tend to decrease the lattice parameter of the aluminium matrix [15]. The unusual increase as observed in the present case, seemingly typical in Al–Si dual-phase alloys, is also considered to be caused by the difference in thermal expansion coefficient between the aluminium matrix and the silicon phase with a diamond structure (the linear thermal expansion coefficient of aluminium is about eight times greater than that of silicon) [16]. The thermal expansion coefficient of the δ-phase with a tetragonal lattice structure which is also dispersed in the aluminium matrix is not expected to differ very much from that of the matrix. In order to keep structural coherence between the aluminium matrix and the silicon particles in the

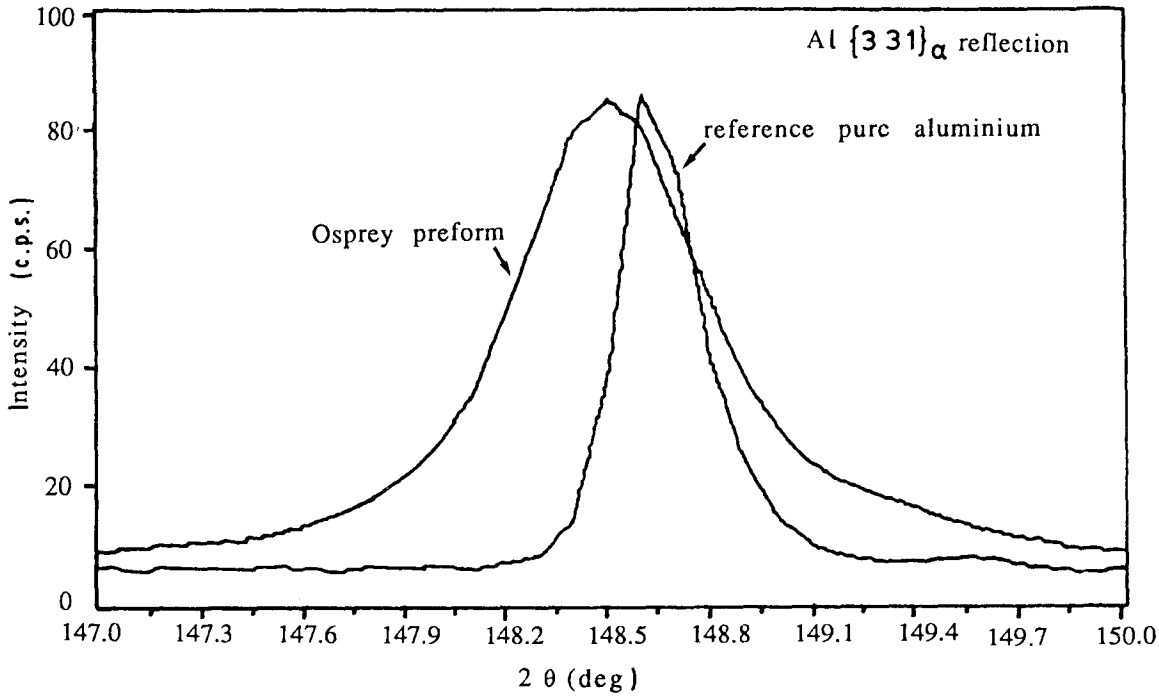

Figure 1 XRD lines as determined from the preform matrix and from pure aluminium.

material cooled from its solidification temperature, tensile stresses were developed in the matrix and thus an increased average lattice parameter of the aluminium matrix was measured. In this case, the usual correlation between the matrix lattice parameters and the amount of solute in the matrix is disturbed, a phenomenon also observed in a melt-spun Al–12Si alloy, which was presumed to have a high level of supersaturation but showed only a marginally lowered matrix lattice parameter [17]. Therefore, for the present Al–Si based alloy, measuring the preform lattice parameter alone is not sufficient to lead to a conclusion about the amounts of the solute atoms in the aluminium matrix. To ascertain this, heating should be applied to the preform to allow possible precipitation to occur, which was undertaken by using DSC analysis in the present investigation and will be discussed later in this communication.

3.1.3. Intermetallic phases

Identification of intermetallic phases in many rapidly solidified aluminium alloys, particularly those highly alloyed, appears to be much more difficult than in their cast counterparts, due to large departures from their equilibrium states. Determining the phase constitution in an aluminium alloy is, however, of great importance for understanding and controlling structures and resultant properties. In the present alloy, undoubtedly, the massive silicon particles constitute a principal dispersion phase which contributes greatly to the unique properties of the material such as low density, excellent wear resistance and low thermal expansion coefficient. To obtain additional strength, especially hot strength, creating a fine, thermally stable intermetallic dispersoid phase (or phases) is essential. XRD revealed the presence of a large amount of the metastable phase, identified as δ-Al_4FeSi_2 (ASTM card 20–33), in the present Osprey preform. An XRD pattern is presented in Fig. 2, which shows that the strong reflection lines from the preform fit the δ-phase standard data very well and the ratios of the reflection intensities are virtually the same. The figure also shows very weak reflections from the equilibrium phase, β-Al_5FeSi (ASTM card: 20–31), coexistent in the preform. The δ-phase has a volume fraction of 15–20% similar to that of the silicon phase, estimated on the assumption that all the iron is consumed in this phase. Apparently, the δ-phase is the second important dispersed phase in the Osprey preform of the alloy. This phase with a shape of thin platelets (needles on sections) should be formed as a primary phase and have been transformed into the β-phase through a peritectic reaction under the equilibrium conditions. Its retention in the present preform clearly indicates the effective suppression of this transformation during the Osprey process and the non-equilibrium state of the as-spray-deposited material, an important characteristic produced by a rapid solidification process. The positive identification of the

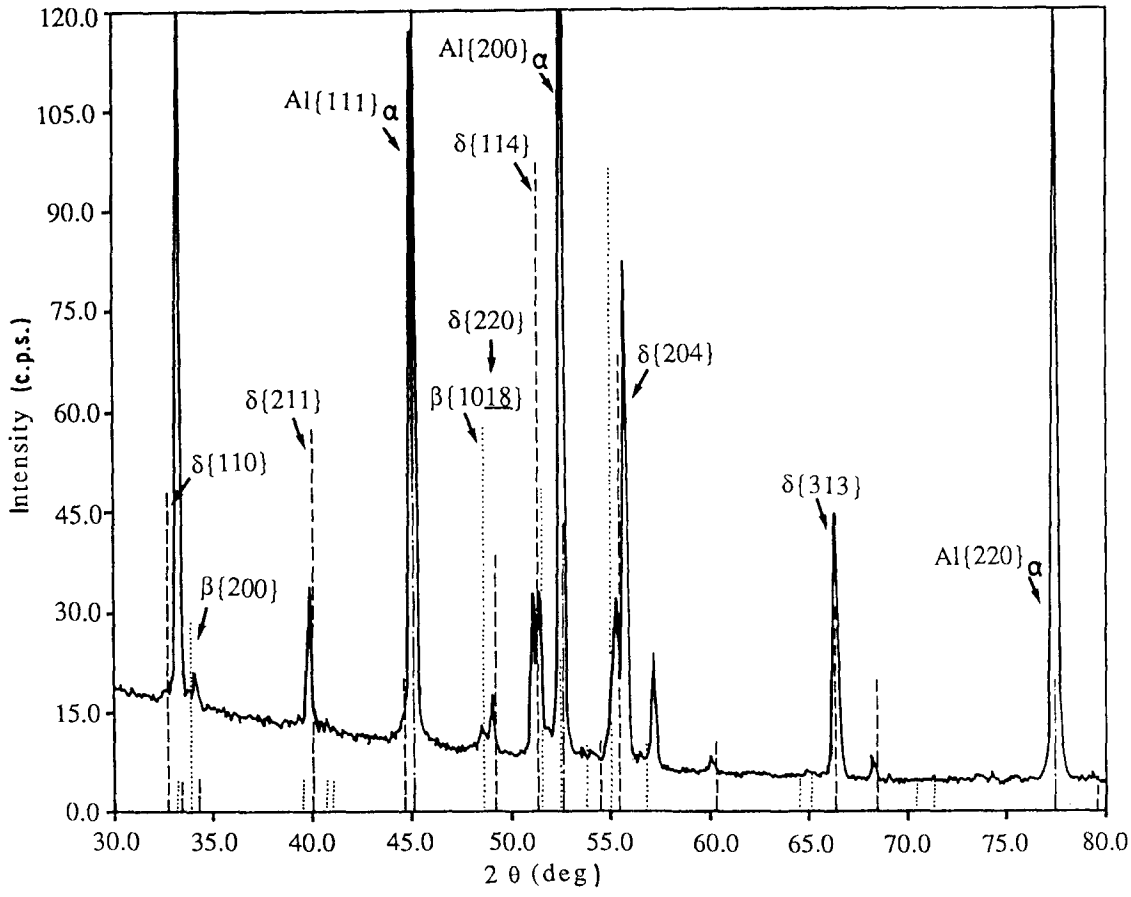

Figure 2 Identification of the metastable δ-phase in the preform. Diffraction patterns of (——) Osprey preform, (—·—) pure aluminium, (– – –) δ-AlFeSi (standard), (···) β-AlFeSi (standard).

δ-phase in the present Osprey Al–20Si–5Fe alloy also suggests that the intermetallic phase with a similar morphology in the powdered Al–20Si–5Fe–3Cu–1Mg alloy [18] should be a variant, possibly with a little involvement of copper and magnesium [19].

3.1.4. Thermal effects

A DSC thermogram is given in Fig. 3, which shows the thermal effects exhibited by the material in the as-spray-deposited condition during heating to 550 °C (the lower curve), and those during reheating to the same temperature (the upper curve). The declination of the dashed lines, defined as base lines to indicate no occurrence of thermal reactions, is due to the difference in heat capacity between the alloy in question and the reference specimen of pure aluminium, which is assumed to be a linear function of temperature. It can be seen from the lower curve (the first heating cycle) that there is no pronounced exothermic spike indicating a precipitation process over the temperature range between 100 and 300 °C where the decomposition of a supersaturated aluminium matrix is expected to occur [20]. Therefore, it is now manifest that there is almost no supersaturation of iron and silicon in the aluminium matrix of the present Osprey preform. At the first glance, this result seems to be in contradiction with the common understanding that the Osprey process involves rapid solidification, one of the common characteristics of which is extending the solid solubility limits of alloying elements in aluminium. However, considering the specific cooling conditions of an Osprey preform, this finding is understandable. During spray deposition, droplets upon their formation are indeed cooled very rapidly through forced convection and radiation as occurring in normal atomization. The exact cooling rates at this stage depend mainly on individual droplet sizes under a given atomizing condition. For the droplets finer than a critical size, high cooling rates enable them to solidify completely during their flight, and considerable degrees of supersaturation and metastable phase formation can be expected in these presolidified droplets. After arriving at the deposition surface, however, they tend to be reheated or probably partially remelted in the semi-liquid/semi-solid mixture so that the previously attained supersaturation will be diminished at the later stages. On the other hand, these presolidified droplets are only a small part of the total liquid, and thus their resultant supersaturation levels can hardly give a significant influence on those of the bulk preform. Most of the droplets arrive at the deposit surface in the semi-liquid/semi-solid state or in the liquid state. The solidification of the remaining liquid proceeds at a rate determined by the removal rate of the heat released due to solidification, mostly through the thermal transfer to the atomizing gas that flows quickly along the surface of the preform. That cooling rate has been estimated to be between 10^2 and 10^4 K s^{-1} [4]. Those droplets successively form a "mushy" layer on the pre-existing deposit. It has been established that in the case of successful functioning of the Osprey process, the "mushy" layer has to be 1–2 mm thick and to contain 10%–40% liquid material [5]. More importantly, the temperature of the layer

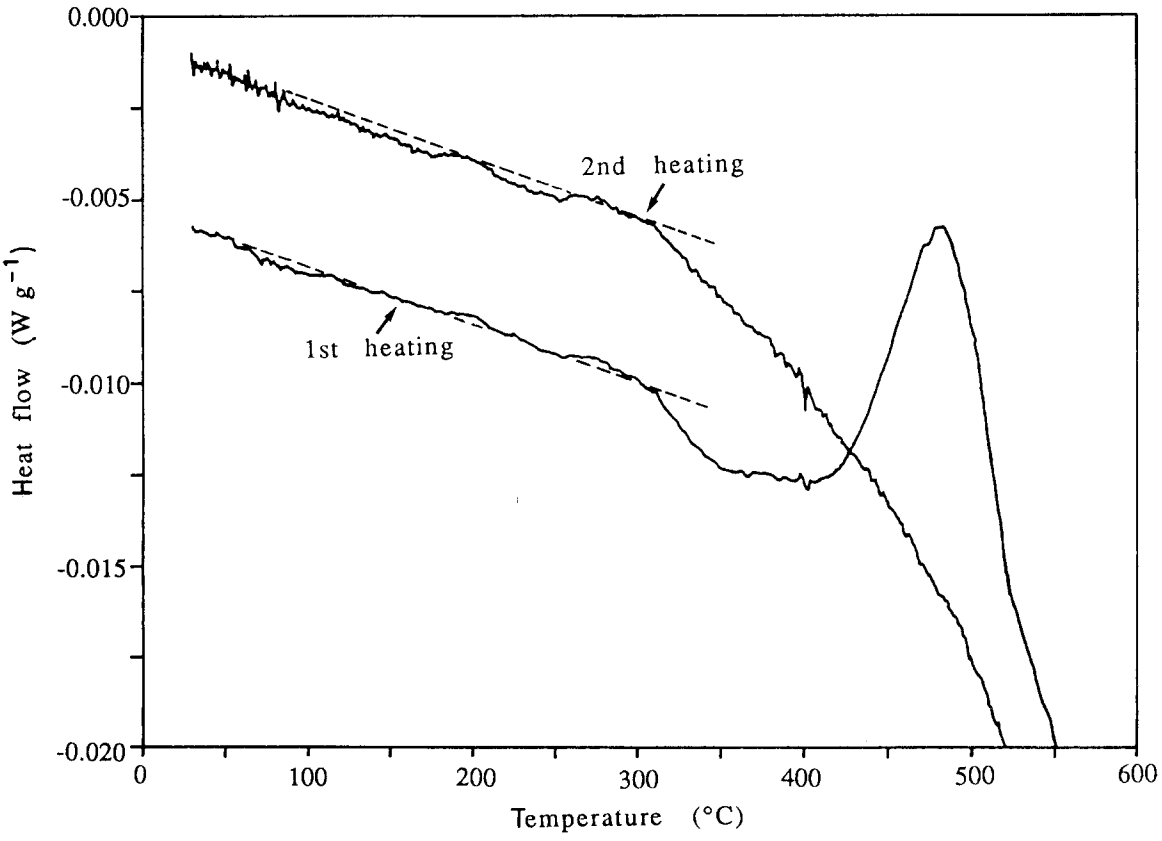

Figure 3 DSC thermogram of the preform.

must be close to the solidus of an alloy being deposited, which obviously facilitates the extensive formation of second phases. According to the Al–Si–Fe ternary phase diagram [19], the equilibrium solidification of the alloy under study starts with the formation of the δ-phase at about 800 °C, followed by the formation of the primary silicon phase at below 700 °C. Below 610 °C the formed δ-phase transforms into the β-phase. At about 576 °C, the ternary eutecticum consisting of the α-matrix, silicon phase and β-phase is reached. It is a well known phenomenon that in undercooled hypereutectic aluminium alloys the formation of a large amount of primary phases can be effectively prevented so that the sequence of equilibrium solidification events cannot be followed. From the appearance of the as-solidified microstructure of the preform with an irregular discontinuous eutectic characteristic, as will be shown later, this also happens in the present alloy and its solidification principally proceeds in a faceted eutectic mode. The observed depletion of the solute atoms in the aluminium matrix is clearly associated with the solidification mode, which will be later described at length with reference to the as-spray-deposited microstructure. Briefly, the formation of the aluminium matrix leads to a great enrichment of solute concentrations in the remaining liquid and finally to the formation of the silicon phase and δ-phase, due to the insufficiently high cooling rate and undercooling level for partitionless solidification offered by the Osprey process and the high driving force for solute partitioning of the alloy. It is very important to note that as the solidification proceeds by forming the aluminium matrix, not only thermal gradients are diminished but also local recalescence occurs. As a result, the temperature of the residual liquid close to the solidification front is increased and undercooling levels are decreased. This favours the rejection of a substantial amount of the solute atoms from the solution to form the dispersed phases. In other words, the supersaturation of the solute atoms in the hypereutectic Al–Si–Fe alloy requires high levels of undercooling, but these are limited by the formation of the leading solid phase. Therefore, the combination of the compositional and undercooling conditions is responsible for the formation of high volume fractions of the dispersed phases as observed and thus an insignificant supersaturation of the solute atoms in the Osprey preform matrix. As a matter of fact, such a phenomenon has been observed in other aluminium alloys produced by other rapid solidification techniques. In atomized Al–Si binary alloys, for example, when the silicon content goes beyond the eutectic composition, the matrix lattice parameter shows a tendency of approaching or even exceeding the lattice parameter of pure aluminium [21]. A similar observation has also been reported in melt-spun Al–Fe alloys that with the increase of iron content from 0.5–3.5% (wt), the matrix lattice parameter remains almost unchanged. An explanation for this observation is that a drainage effect, due to the tendency to the growth of an iron-bearing intermetallic phase, becomes stronger with rising iron content to counteract the entrapment of iron atoms in the solid solution [22]. After solidification, the cooling rate of a deposit becomes low when heat dissipates mainly through heat conduction [6], which has been computed to be 1–10 $K\,s^{-1}$ [6–9]. This permits the solute elements remaining in the aluminium matrix to precipitate out. Therefore, in view of the conditions of solidification and secondary cooling as provided by the Osprey process, finding an insignificant supersaturation level in the hypereutectic Al–Si–Fe alloy is not surprising.

Fig. 3 shows a broad trough (see the lower curve) over the temperature range between 300 and 420 °C, which represents the occurrence of an endothermic reaction. This is considered to be caused largely by the redissolution of the silicon phase in the aluminium matrix, because up to 420 °C, the solubility of silicon is increased to about 0.31% (wt) while the solubility of iron remains extremely low, being about 0.0018% (wt), calculated from the isotherm of the Al–Si–Fe ternary phase diagram at that temperature [23]. However, the apparent heat required for silicon dissolution, estimated by integrating the area bound by the trough in the figure, is lower than the previously calculated energy for silicon precipitation [20]. This clearly stems from the heat release from an overlapping exothermic reaction appearing over the temperature range between 420 and 550 °C, overshadowing the thermal effect from the endothermic reaction (see the lower curve in Fig. 3). A comparison with the DSC trace obtained from the second heating shows that the exothermic reaction starts at about 350 °C and probably lasts up to the temperature of incipient remelting (573 °C), which is not far above the terminating temperature of the analysis (550 °C). Two factors have been considered that can account for this broad spike: the coarsening of the dispersed particles with an accompanying decrease in their surface energy, and the transformation of the metastable δ-phase into the equilibrium β-phase. The latter factor has been confirmed by XRD and appears to be more important. The occurrence of the transformation at such a high temperature demonstrates a high requirement of thermal activation for the δ-phase decomposition. Although the transformation during the slow heating in the present DSC analysis has been exhibited to be centred at 485 °C (Fig. 3), it will be shown later that in the material extruded at a preset temperature of 375 °C and a reduction ratio of 10:1, an increased amount of the β-phase has been observed, which is ascribed to the promoting effect of the deformation (strain-induced transformation).

Fig. 3 also illustrates that the DSC trace recorded from the second heating is situated above that from the first heating. This is the evidence of a change in the heat capacity of the material, probably caused by the phase transformation occurring during the first heating cycle, because the conditions of the analysis are identical. During the reheating over the temperature range below 300 °C, no thermal reactions appeared, just as during the first heating. The starting temperature of silicon redissolution was also identical, which implies that this reaction is reversible, that is, the resolved silicon reprecipitated during the cooling

following the first heating up to 550 °C. During the second heating, the exothermic effect above 350 °C was not observed, which means that the material after the first heating cycle practically attained the equilibrium state, and hence the thermal effect due to the silicon redissolution was no longer disturbed. The continuing redissolution of silicon (and a little iron) up to the eutectic temperature (at 577 °C under the present DSC experimental conditions) is clearly illustrated by the heat absorption in the thermogram. The thermal reactions of the as-spray-deposited material observed in the DSC analysis give instructive information concerning not only the preform structure but also its decomposition behaviour during subsequent processing, which will be of use because, in any processing subsequent to spray deposition, heat or combinations of heat and forces will be exerted on the preform.

3.1.5. As-spray-deposited microstructure

Fig. 4 shows the typical SEM microstructure of the preform on the transverse and longitudinal sections, which is composed of the aluminium matrix, the silicon phase mostly with a granular shape, and the intermetallic phase with a platelet shape. It is of great interest to observe many spherical colonies with a size of 10–20 μm (Fig. 4a and c), characterized by the finer and more densely distributed silicon and intermetallic phases in their interior, see Fig. 4b. TEM could not reveal any boundaries of these colonies. It is very important to recognize that the spherical colonies in the present Osprey preform can only be discerned in microstructural sizes, being completely different from those in the aluminium alloys extruded from powders, which usually contain oxides that outline the original powder particle boundaries. Such a colony-like morphology observed in the present Osprey preform has

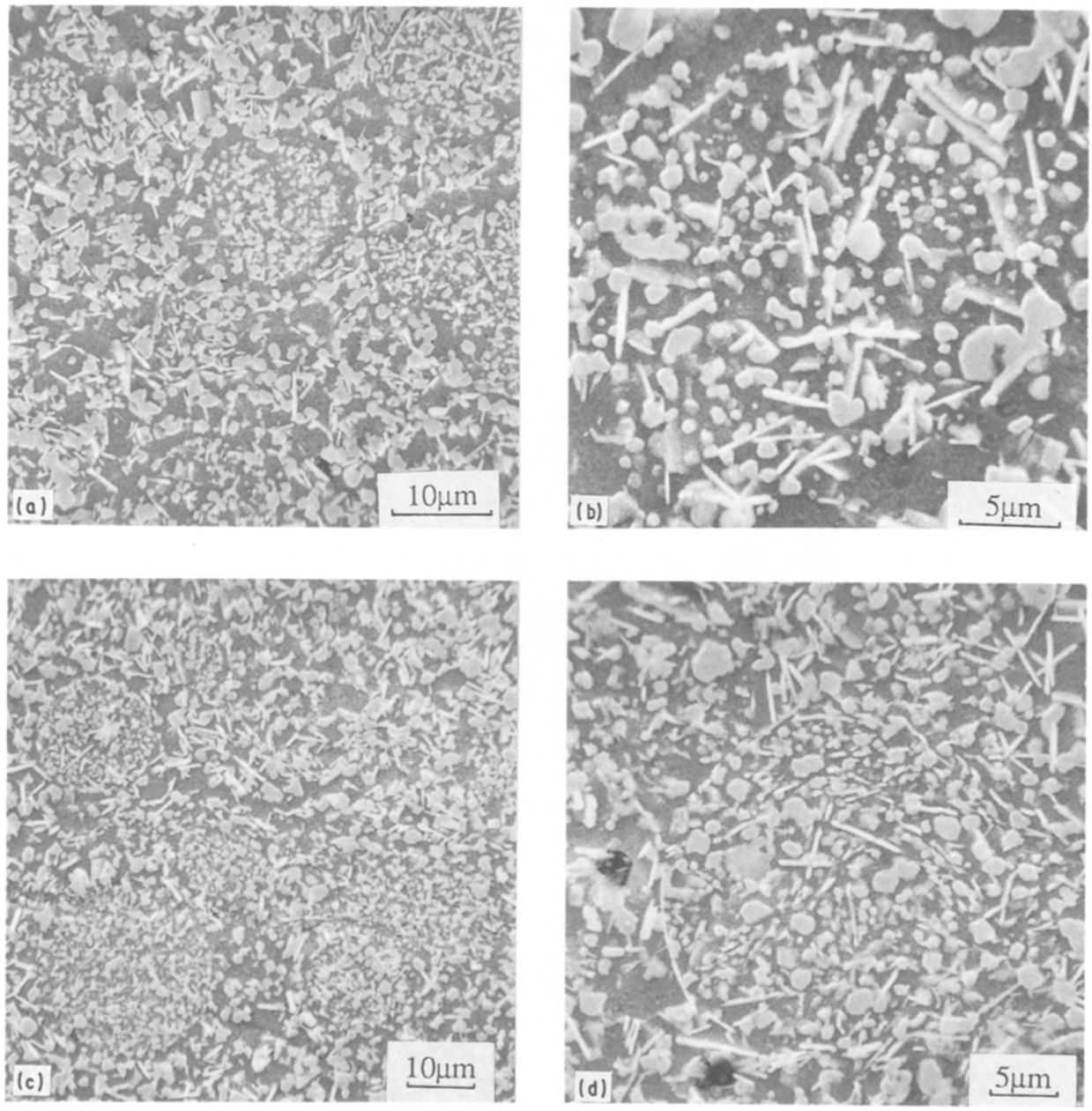

Figure 4 Scanning electron micrographs taken (a, b) from transverse sections, and (c, d) from longitudinal sections of the preform, showing spherical colonies, their structural characteristics and micropores at their peripheries.

not been reported by other investigators. It is obviously associated with the solidification mechanisms of the Osprey process. The difference between the microstructural size inside and outside the colonies clearly shows a transition in cooling rate. As stated earlier, depending on experimental conditions, the droplets finer than a critical size can solidify prior to impingement [6]. While under the ideal conditions of spray deposition, termed as non-particulate mode of deposition, the presolidified droplets tend to be remelted to lose their identity upon deposition [24], in practice the remelting can hardly proceed completely in the top layer of a deposit with 10%–40% liquid material. It is therefore considered that a certain number of the colonies are originated from the remains of the presolidified droplets which may be partially remelted at the deposition surface. However, the presolidified droplets are only a part of the total liquid (which was estimated to be 16% of the total mass for aluminium alloys [6]), and cannot possibly account for the numerous spherical colonies observed in the microstructure. It has been accepted that a substantial number of the droplets are in the semi-liquid state on impingement, which means that a varying volume fraction of solid is already formed in those droplets during flight. The solidification at the early stage can proceed through multiple, heterogeneous nucleation at the surfaces of those droplets as well as in their interior. When impacting the deposit surface at a high velocity, they are crushed, but the already solidified material may retain a spherical shape. The solidification subsequent to deposition can easily proceed outward from these particles until all the liquid in the interstices is solidified, but at a reduced rate depending largely on the external heat transfer. This allows the coarsening of the structure outside the colonies. It is worth mentioning that presolidified material in the large droplets can also be partially remelted when embedded in the semi-liquid mixture, due to the local heat flow from the liquid. The remelting proceeds until local temperature equilibrium is approached, and then the remaining solid material acts as nuclei for solidification. It is also possible that some of the very fine solidified particles are completely remelted upon deposition, as postulated under the ideal deposition conditions, but renewed, heterogeneous nucleation can initiate *in situ* due to favourable, local compositional conditions, because these events take place too quickly to allow the complete redistribution of the solute atoms. Additionally, the possibility of the formation of new nuclei, catalysed by the impacting of flow gas and newly arriving droplets, cannot be ruled out. It is, however, believed that most of the colonies observed in the microstructure of the preform are originated from the remains of the fine droplets and those of the particles in the larger droplets which are solidified at the early stage prior to deposition and then partially remelted upon deposition. The colony-like morphology therefore represents a discontinuity of solidification during the Osprey process.

The microstructural appearance in each colony is very similar to an irregular discontinuous ternary eutectic, consisting of the non-faceted aluminium matrix, the faceted silicon particles and the δ-phase platelets, typically as shown in Fig. 4b. Note that such a eutectic characteristic is completely different from normally observed regular eutectics in terms of the degree of regularity and interspacing between phases. This kind of irregular eutectic has been known in cast Al–Si binary alloys [25] and also found in rapidly solidified Al–Si alloys [26]. The present observation suggests that the irregular eutectic also appears in the ternary alloy produced by the Osprey process. Much larger interspacing between the δ-phase platelets than that between the silicon particles suggests that solidification begins with the binary eutectic reaction of the aluminium matrix and the faceted silicon particles, and is followed by the ternary eutectic reaction when the iron in the liquid is rich enough to form the δ-phase.

On the longitudinal sections (through the height of the preform discs), layering was generally not observable, but occasionally very fine micropores concentrated close to one plane could be found, which appear to result from the spreading of the arriving droplets with entrapped gas beneath. Porosity measurements showed an average value of 1.2% in the preform, which indicates that nearly full consolidation has been accomplished in the Osprey process. Microscopy revealed that the pores had various sizes under 50 μm, and most of them were situated at the peripheries of some of the spherical colonies or at their interstices, see Fig. 4d. This suggests that a main cause of the porosity formation could be the gas entrapped between some arriving droplets and the pre-existing deposit. However, another possibility that the evolution of hydrogen from the feedstock creates micropores can hardly be ruled out and needs to be studied. A close inspection of the micropores showed coarsened silicon particles surrounding them, indicating locally reduced efficiency of heat extraction. Obviously, the micropores present in the material will act as origins of failure, and it is essential to eliminate them by applying plastic deformation so as to obtain desired mechanical properties, fatigue resistance and fracture toughness in particular.

In the as-spray-deposited material, the silicon particles had an average size of 2 μm (as determined by optical microscopy), being a little larger than that in the atomized powder of a similar alloy [18]. However, the platelet-like intermetallic phase (with a needle shape on sections), being randomly distributed in the Osprey preform, was much shorter (only about 2–5 μm long), as can be seen in Fig. 5. There is no evidence to prove that the long platelets of the intermetallic phase formed in flight were fragmented upon impaction on to the top of the pre-existing deposit at a high velocity. More sites of heterogeneous solidification nucleation in the droplets with higher undercoolings offered by the Osprey process are probably a prime factor that limits the growth of the platelets in length to intersection within the colonies which had much finer sizes than most of the powder particles produced by normal atomization [18]. As the platelet-like morphology of the intermetallic phase is generally considered to be unfavourable for good workability,

fatigue properties and fracture toughness [27], it is desired to be broken up by the shear stresses intrinsic to extrusion, which will be discussed later.

Fig. 6 shows the transmission electron micrographs of the as-spray-deposited material, illustrating the silicon phase dispersed in and the platelet-like intermetallic δ-phase intersecting the aluminium matrix with extremely fine cells. Occasionally, very fine precipitates decorate the cell walls, which could not be analysed by using XRD because of their very small sizes and low volume fraction. It can also be seen that in the regions neighbouring the dispersed-δ phase the microcellular feature is substantially absent. This characteristic microstructure accounts for the solidification mechanisms of the alloy during the Osprey process which operate mainly in a faceted eutectic mode. Solidification starts with the aluminium matrix formation at heterogeneous nuclei, because the subsequent silicon phase nucleation by the solid aluminium can more easily proceed in view of relative interfacial energies [28]. As the cooling rates and undercooling levels in the Osprey process are not sufficient to prevent the partitioning of the solute atoms, microsegregation occurs which results in the formation of microcells. As the cellular solidification proceeds, the solute concentrations at the growth front are increased until the liquid is sufficiently enriched in silicon and iron for an incoherent nucleation of the faceted silicon phase and δ-phase. Their formation consumes a large number of solute atoms, giving rise to the depletion of solutes and the absence of matrix microcell walls in their surroundings, as can be observed in Fig. 6. The microcell walls with segregated solutes are decomposed in the solid state by forming precipitates so as to release the supersaturated solute atoms, which can occur either at high temperatures with the aid of recalescence or during the secondary cooling of the deposit. Clearly, the faceted eutectic solidification and the subsequent aluminium matrix decomposition are responsible for the depletion of the solute atoms in the as-spray-deposited aluminium matrix, as shown earlier.

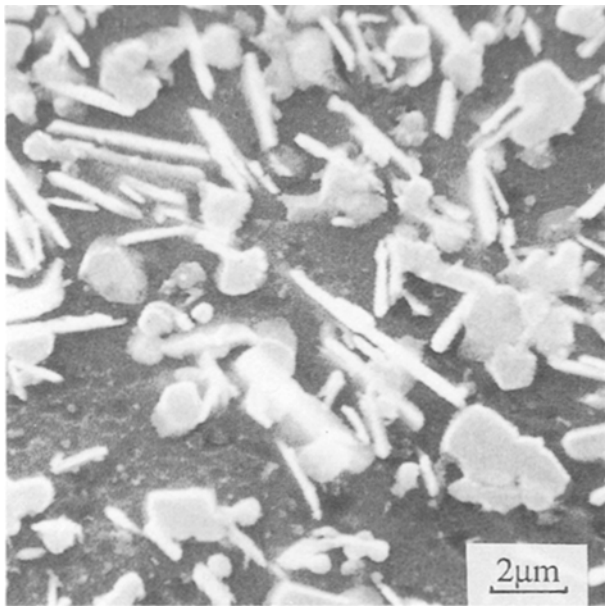

Figure 5 Scanning electron micrograph showing the sizes and morphologies of the silicon phase and δ-phase in the preform.

3.2. Structural evolution during extrusion and annealing

3.2.1. Matrix lattice

XRD lines from the matrix of the material after the extrusion at the temperature of 375 °C and the reduction ratio of 10:1 did not show any noticeable change in breadth, but the relative intensities from major reflection planes were significantly changed due to the influence of the texture induced during the deformation to the as-spray-deposited material with pre-existing texture. Subsequent annealing at 300 and at 400 °C further altered the relative intensities, making them progressively approach those from the reference pure aluminium with random texture, which suggests an

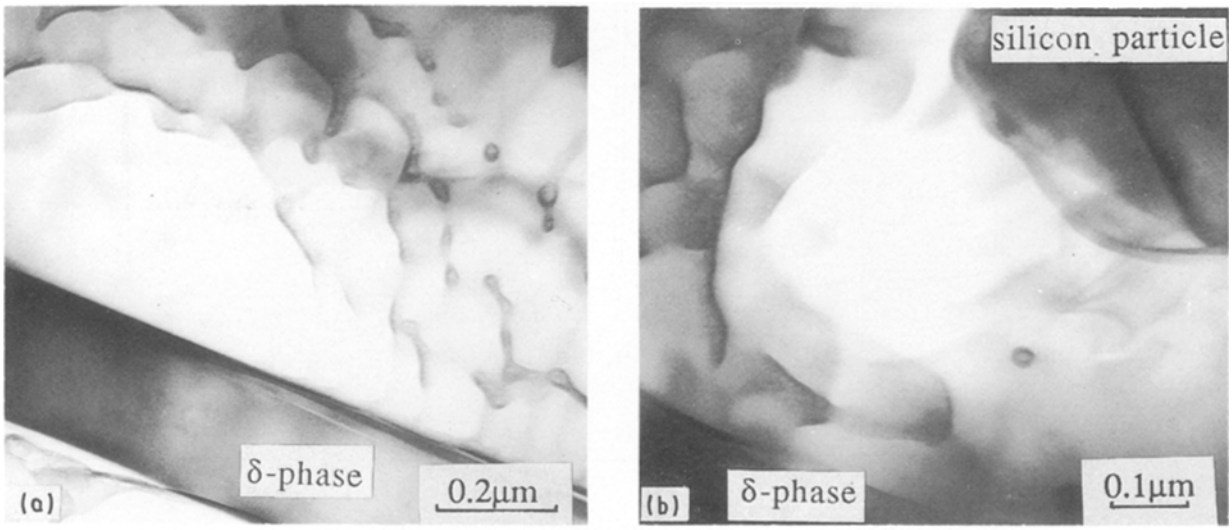

Figure 6 Transmission electron micrographs (a) and (b) showing the platelet-like intermetallic phase and silicon phase present in the matrix of the preform with microcells.

increase in the volume fraction of recrystallized grains with rising annealing temperature. The broadening of the diffraction lines from the as-annealed matrices still existed. It confirms that the lattice strains of the matrices caused by the dispersed silicon phase could not be eliminated by applying annealing [16]. The average lattice parameters of the aluminium matrices of the material in the different states, which were calculated from the high-angle reflections after eliminating the K_{α_2} component, are gathered in Table I. The similar values clearly indicate that the increased lattice parameters (the solutions of silicon and iron within their equilibrium solubility limits practically do not alter the matrix lattice parameter [15]) cannot possibly be caused by the retained solute atoms. It also shows that the matrix structure after spray deposition already approached the equilibrium state and was not altered during further processing.

3.2.2. Intermetallics

XRD analysis revealed the coexistence of the metastable δ-phase and equilibrium β-phase in the extruded material. Of interest is the notable increase in the amount of the β-phase and the corresponding decrease in the δ-phase as compared with the reflections from the as-spray-deposited preform. This is clearly shown in Fig. 7, even though a quantitative comparison was difficult to make. Because the as-spray-deposited aluminium matrix did not contain excess solute atoms, as shown earlier, the increased β-phase must have been transformed from the metastable δ-phase. This solid state phase transformation was, however, almost negligible when the preform was heated in the DSC analysis up to the temperature of 375 °C as preset for the extrusion. It implies that the transformation kinetics was speeded up by the high-rate deformation. This effect can be attributed to the

TABLE I Average lattice parameters of the material measured from the {3 3 1} reflection and at 23 °C

	Peak position (2θ deg)	*d*-spacing (nm)	Lattice parameter (nm)
Osprey preform	148.5040	0.092 936 6	0.405 10
Material extruded at 375 °C/10:1	148.4987	0.092 937 9	0.405 11
Material heated at 300 °C for 100 h	148.4227	0.092 943 8	0.405 13
Material heated at 400 °C for 100 h	148.4907	0.092 939 7	0.405 12
Pure aluminium	148.6299	0.092 907 9	0.404 97

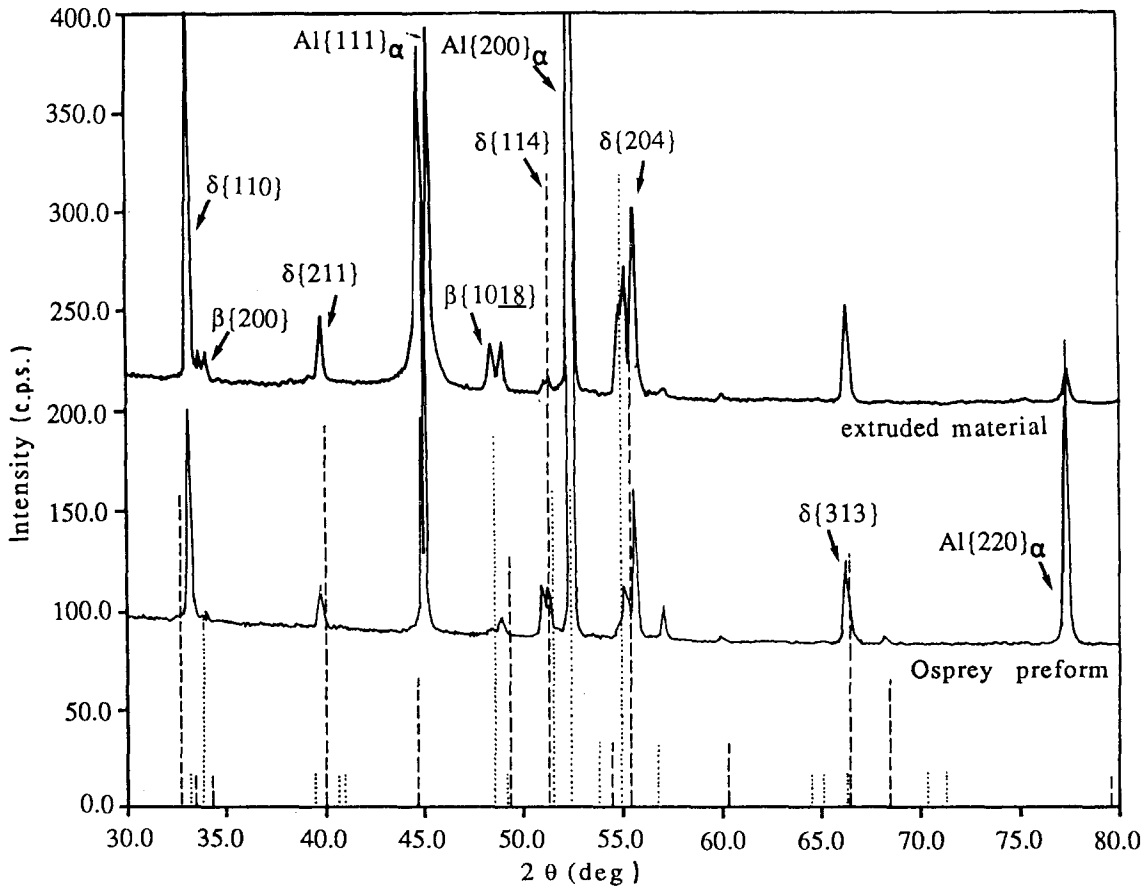

Figure 7 Comparison of the diffraction lines from the Osprey material (——) before and (——) after extrusion at 375 °C/10:1. Standard diffraction patterns: (– – –) δ-AlFeSi, (···) β-AlFeSi.

reduction of the activation energy for the nucleation of the new phase, the creation of vacancies, dislocations and subgrain boundaries which facilitate the atomic diffusion, and the increase of temperature which enhances atomic activities. Nevertheless, it should be noted that in the material extruded under the given conditions, most of the δ-phase was still retained, as indicated by the small reductions of the reflections from that phase. It means that the experimental extrusion conditions did not allow the completion of the transformation, although it was somewhat promoted by the deformation. Based on the DSC and extrusion results, it can be predicted that a large increase in extrusion temperature and deformation rate will bring the transformation to completion. Because the alloy in question is normally non-heat-treatable, the volume fractions of the as-extruded intermetallic phases are very likely to be inherited by the final product. Particular attention should therefore be paid to choosing appropriate process parameters so as to control the intermetallic phases present in the extruded material. Unfortunately, no comparative data are currently available concerning the proper choice of the intermetallic phases to obtain better properties of the alloy with regard to workability and engineering applications.

Because the alloy is designed to be used at elevated temperatures, as in automobile engines and compressors, an understanding of its thermal stability is necessary, which was obtained by exposing the extruded material at 300 and 400 °C for 100 h in the current investigation. The former was considered as a normal temperature and the latter as a possible temperature to be used in service or in secondary forming such as forging in order to reduce loads on tooling. After the exposure at 300 °C, no apparent change was found in the major reflections from both the intermetallic phases, indicating that up to this temperature, the as-extruded metastable δ-phase remained untransformed and hence was thermally stable, in agreement with the DSC results. However, after the heating at 400 °C, the β-phase reflections became stronger and well defined, and some minor δ-phase reflections almost disappeared (see Fig. 8), which implies an increase in the volume fraction of the β-phase. This observation is generally consistent with the results obtained from the DSC analysis which has shown that the transformation starts to occur at about 350 °C. However, in the DSC experiments the bulk of the transformation takes place at much higher temperatures (around 485 °C). It should be noted that the conditions of the annealing treatment applied to the alloy are different from those in the DSC analysis, which may be responsible for the reduced transformation temperature. Firstly, the continuous heating applied in the DSC analysis of the preform at a relatively fast rate (5 °C min^{-1}) pushed the transformation toward a higher temperature. The isothermal annealing of the extruded material for 100 h provided enough time for atomic diffusion. Secondly, the extrusion fragmented the δ-phase from long platelets into short rods, as will be shown below, which

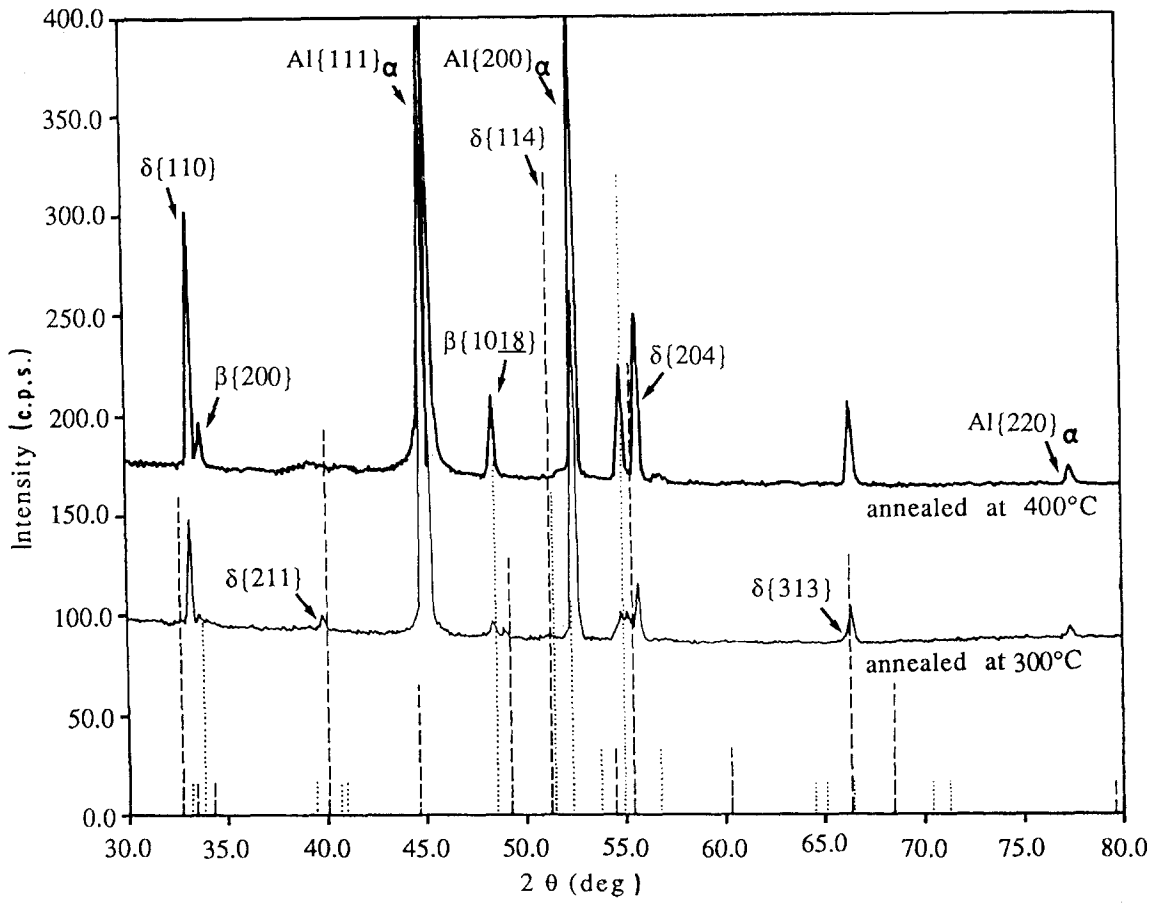

Figure 8 Comparison of the diffraction lines from the material annealed at (——) 300 and (——) 400 °C for 100 h. Standard diffraction patterns as in Fig. 7.

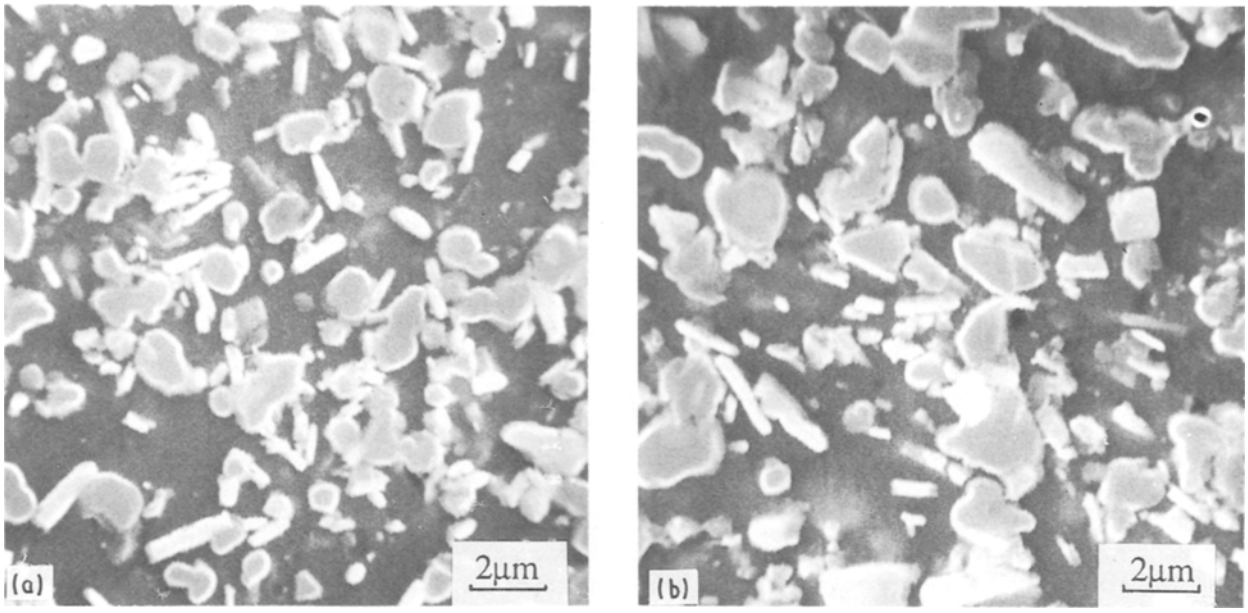

Figure 9 Scanning electron micrographs taken from (a) transverse and (b) longitudinal sections of the extrudate showing the fragmented intermetallic phase and their alignment in the extrusion direction.

considerably enhanced their interface energy and thus reduced their stability. Thirdly, the stored strain energy was not completely released after the extrusion due to the resistance of the material to restoration, and this would assist the transformation. Therefore, the thermal stability of the metastable phase retained in the rapidly solidified material is also related to its processing history.

3.2.3. As-extruded microstructure

As shown earlier from the X-ray diffraction results, a high volume fraction of the metastable δ-phase was retained in the extruded material, but its initial platelet-like morphology (needles on sections) was significantly altered. Fig. 9a and b show scanning electron micrographs taken from the transverse and longitudinal sections of the extrudate, respectively. By comparing them with Fig. 5, it can easily be seen that the initial long platelets were fractured into the short rods with a length of 0.5–2 μm by shear stresses involved in the extrusion deformation. The fragments were generally oriented in the direction of the metal flow. The original spherical colonies could not be recognized in the as-extruded structure, indicating that they were destroyed by the metal flow which redistributed the silicon particles and intermetallic fragments. The original micropores were also eliminated by the extrusion. Therefore, the noticeable characteristics of the material produced by the Osprey process no longer exist after the extrusion and behaviour of the extruded material similar to that produced by other rapid solidification techniques can be expected.

The as-extruded microstructure was homogeneous in optical and SEM images, as typically shown in Fig. 10. However, TEM at high magnifications revealed a non-homogeneous, complex microstructure. The cellular characteristic as seen in the preform was not observable in the extrudate, but a large number of fine,

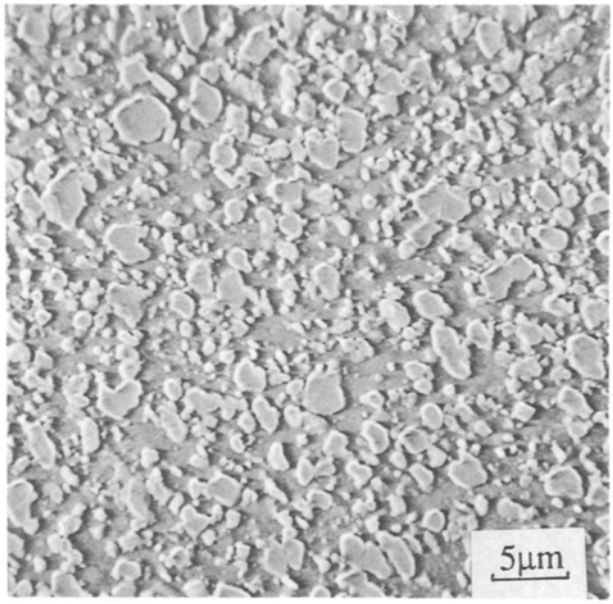

Figure 10 Scanning electron micrograph showing a homogeneous structure after extrusion.

rod-like and granular particles appeared, which were distributed non-uniformly in the matrix. Fig. 11 shows transmission electron micrographs taken from the transverse sections of the extrudate. In some regions, subgrains were formed as shown in Fig. 11a, but dislocations with a high density were present in other regions where many dispersed particles were found, Fig. 11b. This implies that in those regions the rearrangement of dislocations during and after the deformation was inhibited and thus recovery could not be complete. The applied reduction ratio of 10:1 and ram speed of 5 mm s^{-1} give an average deformation rate of 2.7 s^{-1} [29], at which many dislocation tangles are generated which are situated both at grain boundaries and within the grains. Such a deformed structure

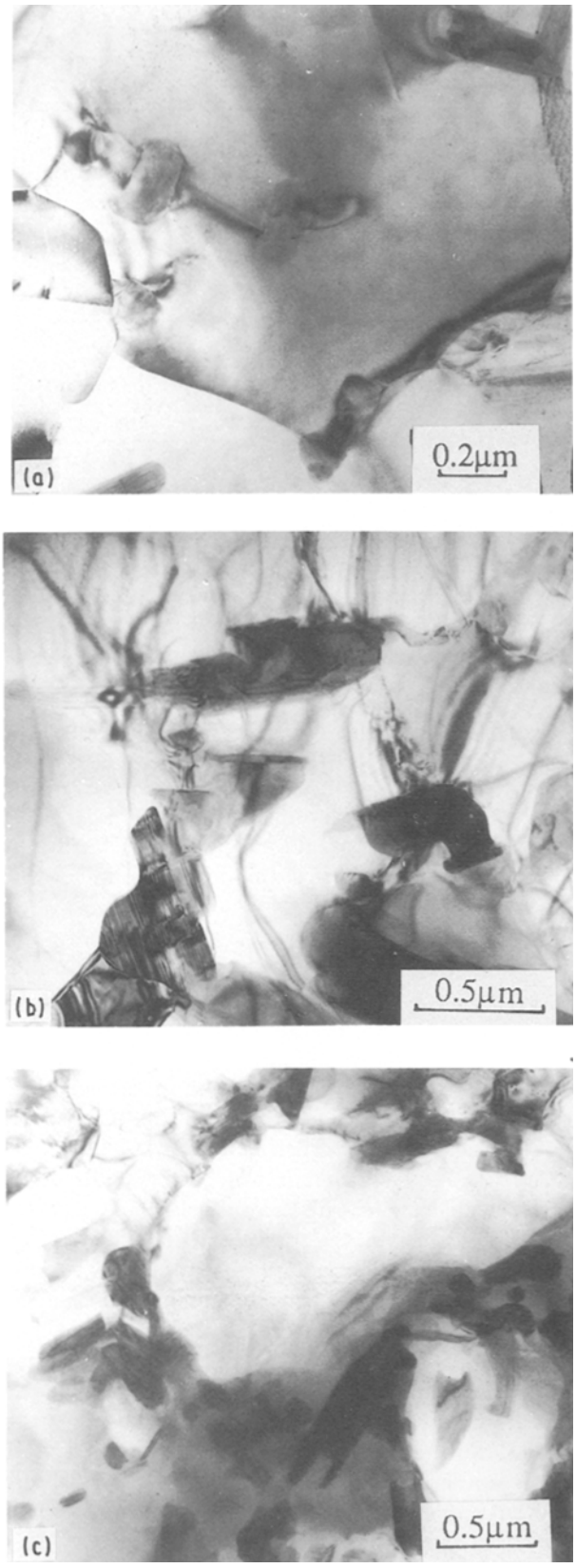

Figure 11 Transmission electron micrographs taken from the transverse sections of the extrudate showing (a) subgrains, (b) dislocation arrays with particles, and (c) recrystallized grains surrounded by particles.

is obviously not thermodynamically stable and thus has a strong propensity to rearranging the dislocation network to a new configuration of lower energy. In the regions where the dispersed particles have a high density, however, the motion of the locked dislocations to the grain boundaries or to form subgrains is difficult and as a result the worked structure is retained. The proceeding of recovery as a principal restoration mechanism in the extruded material, however, does not necessarily exclude the possibility that locally recrystallized grains can be formed. Fig. 11c shows a transmission electron micrograph illustrating recrystallized grains being surrounded by the dispersed particles. It clearly demonstrates that the two restoration mechanisms, namely, recovery and recrystallization, can operate independently throughout the extrudate. The strain energy produced by the high-rate deformation can be released by recovery. But at such locations as subgrain boundaries and the interfaces between the non-deformable, unbroken particles and the aluminium matrix where high misfits are introduced by the deformation of the bulk material, recrystallization can possibly intervene. The recrystallized grains were also observed on the longitudinal sections of the extrudate. Fig. 12a shows a nucleus of recrystallization which might originate at the subgrain boundary junction or at the nearby particles. The nucleus with high-angle misorientation, indicated by sharp contrast to the neighbouring grains, is growing into the surrounding subgrains which have undergone recovery. Because the material was cooled in air after the extrusion, the recrystallized grains could be formed either dynamically or statically. The latter, however, has a higher possibility because of the absence of interior dislocations in the new grains. It should be stressed that despite the presence of some recrystallized grains, the extruded material has principally a recovered microstructure. The longitudinal observation gives some typical characteristics of the extruded material. Fig. 12b shows a banded structure which is composed of elongated grains with different densities of the interior particles being aligned in the extrusion direction. These particles play a very influential role in the internal structure of the grains. In particle-depleted grains, only very indistinct traces of dislocation tangles or subgrains can be seen, indicating that in these regions, dislocations can move relatively freely to interact, allowing annihilation, or move to the sinks such as grain and subgrain boundaries. In the regions with densely distributed particles, however, the mobility of dislocations is substantially reduced. A close inspection could reveal the interlocking of dislocations and the particles aligned in the direction of extrusion, as can clearly be seen in Fig. 12c. It is thus clear that the inhomogeneity of the as-extruded microstructure is largely caused by the non-uniform distribution of the dispersed particles in the aluminium matrix that determine the ease with which dislocations can move.

3.2.4. As-annealed microstructure

As shown above, the as-extruded structure of the material has not attained the equilibrium state and will be further restored, provided that temperature and time allow so. Annealing the extruded material at 300 °C for 100 h led to an increased number of isolated recrystallized grains, as typically shown in Fig. 13a.

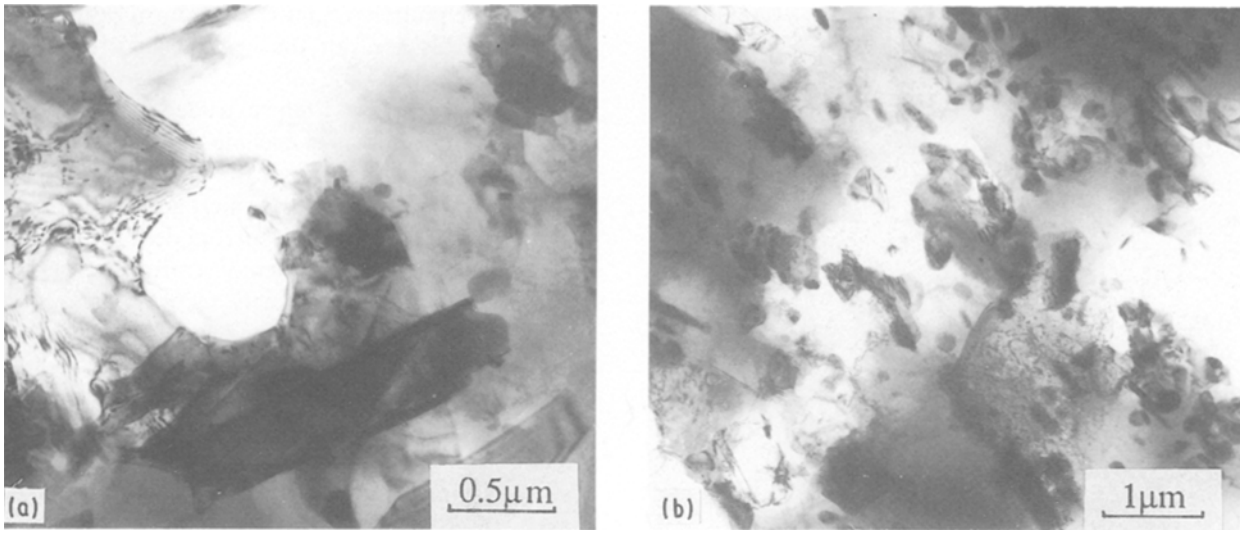

Figure 12 Transmission electron micrographs taken from the longitudinal sections of the extrudate showing (a) a recrystallized grain formed inside a deformed grain, (b) a banded structure, and (c) association of dislocations with the particles aligned in the extrusion direction.

However, their growth into the deformed grains was obstructed by the massive particles in the aluminium matrix (see Fig. 13b). Dislocation tangles with a high density as observed in the extruded material (Fig. 11b) could not be found, indicating that they overcame the pinning of the particles during the annealing. Many equiaxed subgrains were formed, but their boundaries were not always sharpened (Fig. 13c), particularly at those boundaries where particles were located. Fig. 13d shows a low-angle boundary triple junction consisting of ordered dislocation arrays associated with a high density of particles. A possible cause for the observed dislocation arrays is the pinning effect of the particles that inhibit the interaction of the neighbouring dislocations. Another cause could be the difference in thermal shrinkage between the particles and the aluminium matrix that results in thermal strains on the aluminium matrix side. The subgrain size in the annealed material was not uniform because of the differing inhibition of subgrain boundary migration exerted by the high volume fractions of particles non-uniformly distributed throughout the aluminium matrix. In general, the prolonged soaking at the temperature of 300 °C which is above $0.5T_m$ (where T_m is the melting point in K) only helped the resumption of recovery which did not proceed fully after the extrusion deformation, and the microstructure of the material was still principally recovered in spite of the presence of some localized, recrystallized grains.

After the isothermal annealing at 400 °C, the volume fraction of recrystallized grains was further increased and they exhibited well-defined boundaries, as shown in Fig. 14a. It was also noted that most of the new grains were situated inside the deformed grains, suggesting that they were not formed by the migration of original grain boundaries. The growth of the recrystallized grains was still difficult, as can be seen in Fig. 14b which shows the size of a recrystallized grain being restricted to the interspacing of the inhibiting particles. It was previously observed that the worked microstructure of a powder metallurgy Al–20Si–5Fe–3Cu–1Mg alloy was not completely recrystallized after being heated up to 470 °C for 1 h [30]. The present result indicates that the prolonged soaking could not bring the deformed structure to a completely restored state either, probably because a saturation state of recrystallization was attained. Therefore, the observed recrystallization behaviour of the present aluminium alloy containing high volume fractions of particles cannot be described by the conventional kinetics of recrystallization which states that the recrystallization is an isothermal process and the fraction of the recrystallized volume is a function of time above the recrystallization temperature [31].

In the microstructure of the material after annealing, the amount of β-phase was apparently increased, but a systematic coarsening of the intermetallics could not be found. The β-phase, being finer than the retained δ-phase was generally not visible with optical microscopy. Fig. 15 shows the thermal stability of the silicon phase and the retained δ-phase in the material annealed at the given temperatures for 100 h, as determined by optical microscopy. It can be noted that the retained δ-phase remains stable over the range of annealing temperatures, while the silicon

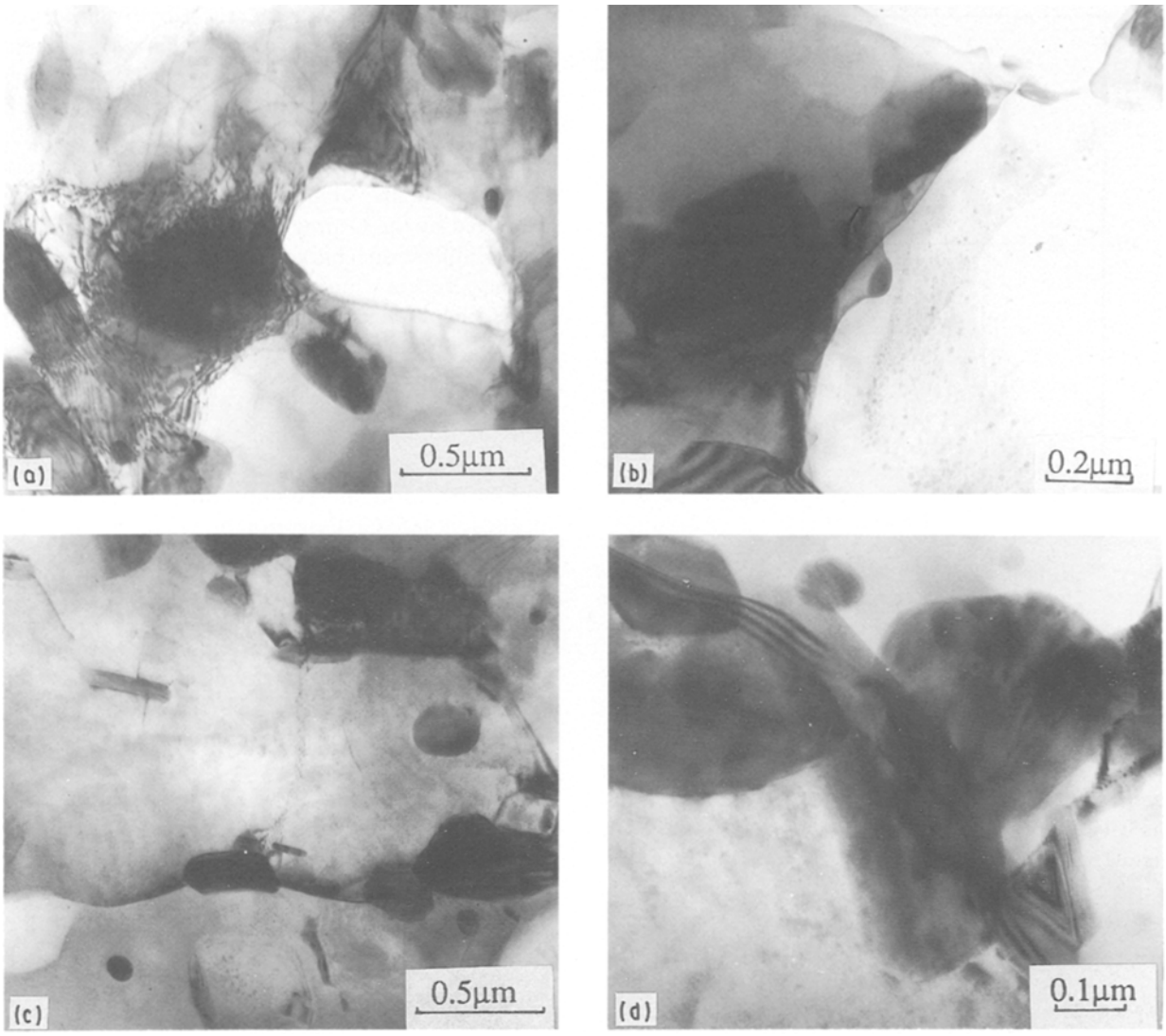

Figure 13 Transmission electron micrographs taken from the material annealed at 300 °C for 100 h, showing (a) an isolated, recrystallized grain, (b) growth of a recrystallized grain being stopped by particles, (c) association of particles with subgrain boundaries, and (d) interaction of subgrain boundaries and particles.

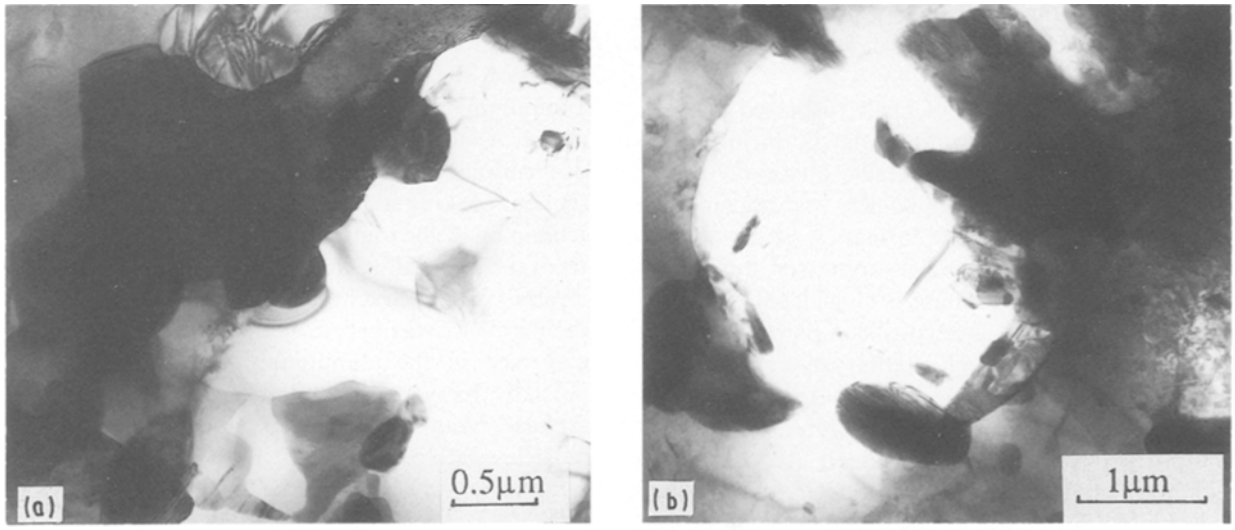

Figure 14 Transmission electron micrographs taken from the material annealed at 400 °C for 100 h, showing (a) a well-defined high-angle grain boundary after recrystallization, and (b) a recrystallized grain within the interspacing of the particles in a deformed grain.

particles are coarsened at 400 °C, which is clearly due to the higher diffusivity of silicon atoms in the aluminium matrix. At this temperature, the silicon particles are able to coalesce through bulk diffusion, grain-boundary diffusion and pipe diffusion. Another cause for the coarsening could be the reprecipitation of silicon which was resolved at the soaking temperature from initially finer silicon particles with relatively high

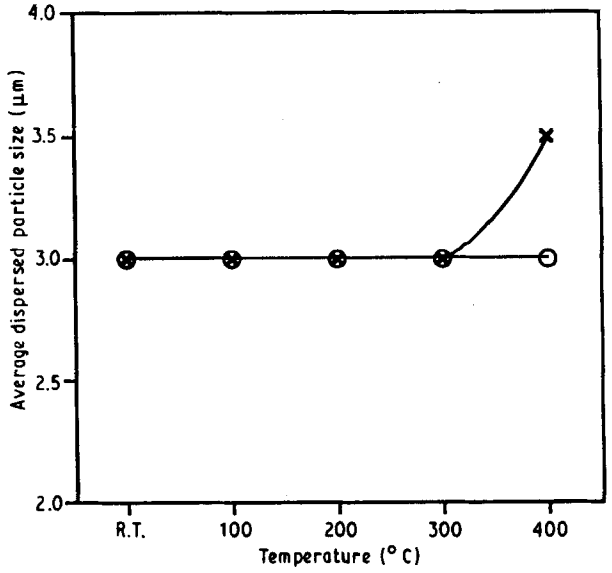

Figure 15 Thermal stability of the silicon phase and the retained δ-phase in the material annealed at each temperature for 100 h. (○) Intermetallic particle size, (×) silicon particle size.

surface energies, at the existing, larger silicon particles during the subsequent cooling. Therefore, the extruded material should preferably not be used at the temperatures above 400 °C where the coarsening of the silicon particles and the transformation of the metastable δ-phase occur.

4. Conclusions

1. The Al–20Si–5Fe alloy preform produced by the Osprey process contained only 0.015% oxygen on average, much less than the material produced by the conventional powder metallurgy. Measurements of porosity showed an average value of 1.2%, and microscopy revealed that the sizes of the pores were finer than 50 μm and that they were situated at the peripheries of spherical colonies. The micropores were eliminated through the extrusion at a reduction ratio of 10:1.

2. Two different kinds of finely dispersed particles were formed in the aluminium matrix during solidification: a metastable intermetallic phase, defined as δ-Al_4FeSi_2, with a shape of platelets, and silicon phase with a granular shape. The formation of the equilibrium β-phase was effectively suppressed during the Osprey process. The δ-phase is considered to be formed together with the faceted silicon particles and the aluminium matrix through a ternary eutectic reaction, according to the irregular discontinuous eutectic characteristic of the preform microstructure. A significant amount of the δ-phase was retained in the material having undergone extrusion at 375 °C and annealing at 300 and 400 °C, but its morphology was changed from platelets into short rods by the shearing involved in extrusion deformation.

3. XRD analysis of the preform exhibited broadened and shifted reflections from the aluminium matrix, which could be attributed mainly to the microstrain resulting from the difference in thermal shrinkage between the dispersed silicon phase and the aluminium matrix. The unusual increase of the lattice parameter of the aluminium matrix persisted throughout the processing applied in the present experiments, suggesting an insignificant effect of the dissolved atoms on the aluminium matrix lattice parameter. DSC analysis confirmed that there was almost no supersaturation in the aluminium matrix of the preform produced by the Osprey process. This is explained by the solidification characteristics of the alloy in the Osprey process which allows the extensive formation of the silicon phase and δ-phase at high temperatures and the further decomposition of the solid solution during secondary cooling.

4. DSC analysis revealed the commencement of the redissolution of the silicon phase at 300 °C and more importantly the decomposition of the metastable δ-phase to form the equilibrium β-phase at 350 °C (peaked at 485 °C). Extrusion at 375 °C resulted in an increased amount of the β-phase, which is considered to be assisted by the high-rate deformation. Annealing at 400 °C subsequent to the extrusion further brought about the formation of the β-phase, largely due to the fragmentation and thus destabilization of the retained δ-phase. The importance of choosing appropriate extrusion conditions is thus emphasized in order to control the phase constitution of the material.

5. The microstructure of the preform showed numerous spherical colonies with sizes of 10–20 μm and finer internal dispersed phases. They are considered to be the remains of presolidified droplets of very fine sizes and presolidified material in the larger droplets, after being partially remelted at the deposition surface. The observed morphology suggests a discontinuity of solidification during spray deposition. Extrusion deformation destroyed the colonies and redistributed the silicon phase and the retained δ-phase.

6. Very fine microcells with precipitates at their walls were observed in the as-spray-deposited aluminium matrix, which are attributable to the characteristics of solidification and subsequent decomposition of the alloy during the Osprey process. After the extrusion, the microcells disappeared. The as-extruded aluminium matrix was inhomogeneous, being composed of subgrains, sometimes with high density of dislocations, and isolated, recrystallized grains. Subsequent soaking at 300 °C for 100 h annealed out the remaining dislocations and allowed the resumption of recovery. Annealing at 400 °C brought about an increased volume fraction of recrystallized grains, but their growth was generally impeded by the particles dispersed in the aluminium matrix, resulting in a partially recrystallized microstructure. The retained δ-phase remained thermally stable, but the silicon particles were coarsened after the exposure at 400 °C for 100 h.

Acknowledgements

The authors thank Osprey Metals Ltd, UK, for supplying the preform used in this work. Thanks are also due to Ing. N. M. van der Pers, Drs M. J. Starink and Ing. E. J. A. van Dam for their help with XRD, DSC and SEM analyses, respectively. The financial support

of the Program of Innovative Research (IOP) in the Netherlands is gratefully acknowledged.

References

1. A. G. LEATHAM, R. G. BROOKS and M. YAMAN, in "Modern Developments in Powder Metallurgy", Vol. 15 (MPIF, New Jersey, 1985) p. 157.
2. Osprey Metals Ltd, UK Pat. 147239.
3. G. J. MARSHALL, in "Proceedings of the International Conference on Aluminium Technology '86", London, March 1986, edited by T. Sheppard (The Institute of Metals, London, 1986) p. 679.
4. J. L. ESTRADA and J. DUSZCZYK, *J. Mater. Sci.* **25** (1990) 1381.
5. P. MATHUR, S. ANNAVARAPU, D. APELIAN and A. LAWLEY, *J. Metals* **41** (1989) 23.
6. E. J. LAVERNIA, *Int. J. Rapid Solid.* **5** (1989) 47.
7. E. J. LAVERNIA, E. M. GUTIERREZ, J. SZEKELY and N. J. GRANT, *ibid.* **4** (1988) 89.
8. E. GUTIERREZ-MIRAVETE, E. J. LAVERNIA, G. M. TRAPAGA and J. SZEKELY, *ibid.* **4** (1988) 125.
9. E. GUTIERREZ-MIRAVETE, E. J. LAVERNIA, G. M. TRAPAGA, J. SZEKELY and N. J. GRANT, *Metall. Trans.* **20A** (1989) 71.
10. R. W. EVANS, A. G. LEATHAM and R. G. BROOKS, *Powder Metall.* **28** (1985) 13.
11. R. H. BRICKNELL, *Metal. Trans.* **17A** (1986) 583.
12. N. AMANO, Y. ODANI, Y. TAKEDA and K. AKECHI, *Metal Powder Rep.* **44** (1989) 186.
13. J. ZHOU and J. DUSZCZYK, in "Hot Deformation of Aluminium Alloys", Proceedings of the 1990 TMS Fall Meeting, "A Symposium on Hot Deformation of Aluminium Alloys", Detroit, Michigan, USA, October 1990, edited by T. G. Langdon, H. D. Merchant, J. G. Morris and M. A. Zaidi (TMS, Warrendale, PA, 1991) p. 473.
14. P. VAN MOURIK, Th. H. De KEIJSER, N. M. van der PERS and E. J. MITTEMEIJER, *Scripta Metall.* **22** (1988) 1547.
15. L. F. MONLDOFO, "Aluminium Alloys, Structure and Properties" (Butterworths, London, 1976) pp. 282, 759.
16. E. J. MITTEMEIJER, P. VAN MOURIK and TH. H. DE KEIJSER, *Phil. Mag. A* **43** (1981) 1157.
17. S. PAIDASSI and J. CHEVRIER, in "Rapidly Quenched Metals", Vol. 1, Proceedings of the Fifth International Conference on Rapidly Quenched Metals, Würzburg, Germany, September 1984, edited by S. Steeb and H. Warlimont (North-Holland, Amsterdam, 1985) p. 957.
18. J. ZHOU, J. DUSZCZYK and B. M. KOREVAAR, *J. Mater. Sci.* **25** (1991) 824.
19. H. W. L. PHILLIPS and M. P. C. VARLEY, *J. Inst. Metals* **69** (1943) 317.
20. M. VAN ROOYEN, PhD thesis, Delft University of Technology, The Netherlands (1988).
21. I. YAMAUNCHI, I. OHNAKA, S. KAWAMOTO and T. FUKUSAKO, *Trans. Jpn. Inst. Metals* **27** (1986) 187.
22. B. BADAN, M. MAGRINI and E. RAMOUS, *Scripta Metall.* **23** (1989) 2121.
23. V. G. RIVLIN and G. V. RAYNOR, *Int. Metals Rev.* **26** (1981) 133.
24. A. G. LEATHAM, A. J. W. OGILVY and P. F. CHESNEY, in "Modern Developments in Powder Metallurgy", Vol. 19, edited by P. U. Gummerson and D. A. Gustafson (MPIF, New Jersey, 1988) p. 475.
25. W. KURZ and D. J. FISHER, *Int. Metals Rev.* **24** (1979) 177.
26. B. A. MUELLER, J. J. RICHMOND and J. H. PEREPEZKO, in "Rapidly Quenched Metals", Vol. 1, Proceedings of the Fifth International Conference on Rapidly Quenched Metals, Würzburg, Germany, September 1984, edited by S. Steeb and H. Warlimont (North-Holland, Amsterdam, 1985) p. 47.
27. Y. TAKEDA, T. HAYASHI, Y. DANI, N. AMONO and N. KUROISHI, personal communication, Sumitomo Electric Industries Ltd, Hyogo, Japan.
28. K. KOBAYASHI, P. H. SHINGU, H. KANBARA and R. OZAKI, *Trans. Jpn. Inst. Metals* **17** (1976) 545.
29. J. ZHOU and J. DUSZCZYK, *J. Mater. Shaping Technol.* **6** (1989) 241.
30. J. ZHOU, J. DUSZCZYK and B. M. KOREVAAR, *J. Mater. Sci.*, in press.
31. M. P. ANDERSON, in "Annealing Process – Recovery, Recrystallization and Grain Growth", Proceedings of the 7th Risø International Symposium on Metallurgy and Materials Science, Roskilde, Denmark, September 1986, edited by N. Hansen, D. Juul Jensen, T. Leffers and B. Ralph (Risø National Laboratory, Roskilde, Denmark, 1986) p. 15.

Received 21 November 1990
and accepted 24 January 1991